Constraint Release in Star/Star Blends and Partial Tube Dilation in Monodisperse Star Systems

Hiroshi Watanabe,* Toshiaki Sawada, and Yumi Matsumiya

Institute for Chemical Research, Kyoto University, Uji, Kyoto 611-0011, Japan

Received January 4, 2006; Revised Manuscript Received February 7, 2006

ABSTRACT: The molecular picture of partial dynamic tube dilation (partial-DTD) was tested for monodisperse high-*M* star polyisoprenes (PI) with the number of entanglements per arm, $N_a = 12$ and 16. To achieve this test on an experimental basis, linear viscoelastic measurements were made for entangled binary blends of these high-*M* star PI in matrices of lower-*M* star PI having $N_a = 2-8$. In the blends, the high-*M* star PI was dilute and entangled only with the lower-*M* matrix stars. Constraint release (CR) relaxation process was viscoelastically detected for those dilute high-*M* stars. The terminal CR mode was close to that expected for the Rouse relaxation of a tethered chain, and the terminal CR relaxation time at 40 °C was described by an empirical equation, $\langle\tau_{CR}^{[2]}\rangle/s \cong 4.0 \times 10^{-5} N_{a2}^2 \exp(0.71 N_{a1})$ with N_{a1} and N_{a2} being the number of entanglement segments per arm of the matrix and probe chains. These $\langle\tau_{CR}^{[2]}\rangle$ data were extrapolated to the monodisperse systems of the high-*M* stars (where $N_{a1} = N_{a2}$) to give the longest CR relaxation time $\tau_{CR}^{[2m]}$ in these systems, and the $\tau_{CR}^{[2m]}$ data were utilized to estimate the maximum possible number $\beta^*(t)$ of entanglement segments at time *t* that were mutually equilibrated through the Rouse−CR mechanism. The corresponding normalized viscoelastic relaxation function for the partial-DTD process, $\mu_{p-DTD}(t) = \varphi'(t)/\beta^*(t)$ with $\varphi'(t)$ being the dielectrically evaluated survival fraction of the dilated tube, was close to the $\mu(t)$ data, suggesting that the partial-DTD picture serves as a good starting point for describing the entanglement dynamics of monodisperse stars.

1. Introduction

In the current tube model representing the entanglement constraint for a focused chain (probe) as the tube, the tube and probe therein change the conformation when the tube-forming chains (matrix chains) diffuse away.[1,2] This tube/probe motion is cast in two different but related molecular pictures. In the first picture referred to as the *constraint release*[1−5] (CR), the entanglement segment of the size *a* and the molecular weight M_e is utilized as the motional unit of the probe and the tube diameter is taken to be identical to *a* in any time scale. The probe exhibits lateral hopping over a distance $\sim a$ when an entangling matrix chain diffuses away to make a hole on the tube, and accumulation of this local CR hopping results in a large-scale motion of the probe.

Because of this accumulation, a length scale of the lateral motion allowed for the entanglement segments of the probe, $a'(t)$, increases with the time scale *t*. In the second molecular picture, this $a'(t)$ is treated as a coarse-grained length scale in the description of the probe motion.[1,2,6] Namely, successive $\beta(t)$ $(= \{a'(t)/a\}^2)$ entanglement segments of the probe are mutually equilibrated through their CR motion to behave as an enlarged segment of the size $a'(t)$, and this enlarged segment is utilized as the motional/stress-sustaining unit of the probe. Correspondingly, the tube has an effective diameter $a'(t)$ that dynamically dilates with *t*. In this picture referred to as the *dynamic tube dilation*[1,2,6−11] (DTD), the enlarged segments of the probe are allowed to move only *along* the dilated tube axis. This treatment smears detailed dynamics in the accumulation of local CR hopping (increase of a') but greatly simplifies the description of the probe motion.

Most of the current tube models make an additional assumption that the relaxed portions of the probe and matrix chains behave as a simple solvent.[6−11] With this assumption, the number of the entanglement segments per enlarged segment, $\beta(t) = \{a'(t)/a\}^2$, *fully* increases to the number determined by the tube survival fraction $\varphi'(t)$ (= fraction of the nonrelaxed portion), $\beta_{f-DTD}(t) = \{\varphi'(t)\}^{-d}$ ($d = 1-1.3$; dilation exponent). In this *full-DTD* molecular picture, the normalized viscoelastic relaxation function $\mu(t)$ is simply written in terms of $\varphi'(t)$ as[6−11]

$$\mu_{f-DTD}(t) = \varphi'(t)/\beta_{f-DTD}(t) = \{\varphi'(t)\}^{1+d} \qquad (1)$$

Here, the factor $1/\beta_{f-DTD}(t)$ represents a magnitude of the stress decay due only to full-DTD (= the decrease in the total number of the stress-sustaining units due to enlargement of these units). The models based on this full-DTD picture describe the viscoelastic data of monodisperse linear and star chains with a remarkable accuracy.[7−9] However, the viscoelastic data just reflect a particular aspect of the chain motion (decay of orientational anisotropy), and the success of the full-DTD models does not necessarily guarantee that the real chains move in the way assumed in these models.

To test the validity of the full-DTD picture, we recently focused on the dielectric behavior of *cis*-polyisoprene (PI) having the electrical dipoles parallel along the chain backbone.[12−19] From the dielectric data of PI (detecting the orientational memory decay), we evaluated the tube survival fraction $\varphi'(t)$ without relying on any particular model. Comparing $\mu_{f-DTD}(t)$ calculated from this $\varphi'(t)$ (eq 1) with the $\mu(t)$ data, we found that the full-DTD picture works well for monodisperse linear chains[12,15−17] but fails for monodisperse stars[13−15,17] and linear/linear blends,[12,18,19] the latter having a relatively small volume fraction v_2 of a high-molecular weight (*M*) component.

The failure of the full-DTD picture for the stars, noted also in the analysis of the self-diffusion coefficient,[20] is related to their intensive fast relaxation modes: These modes lead to a significant increase of the full-DTD length scale $a_{f-DTD}'(t) =$

* To whom correspondence should be addressed. E-mail: hiroshi@scl.kyoto-u.ac.jp.

10.1021/ma0600198 CCC: $33.50
Published on Web 03/14/2006

$a\{\varphi'(t)\}^{-d/2}$ (decrease of φ') at short t before the terminal relaxation occurs. The CR-equilibration cannot be completed in time over such a large scale, which results in the severe failure of the full-DTD picture for the stars in the terminal regime.[15] Similarly, in the linear/linear blends with small v_2, the intensive fast modes of the low-M component give a large increase of $a_{f-DTD}'(t)$ and the CR-equilibration over this $a_{f-DTD}'(t)$ cannot occur for the high-M component at intermediate t, which results in the failure of the full-DTD picture at those t.[18,19] This failure was noted also for star/linear blends at intermediate t.[10] (Correspondingly, the success of this picture for the monodisperse linear chain systems is related to the lack of intensive fast modes in these systems.[15])

The failure of the full-DTD picture indicates that the relaxed portions of the chains are *not always* equivalent to a simple solvent. At the same time, the failure does not rule out the DTD process itself over a length scale $< a_{f-DTD}'(t)$: The tube undoubtedly changes its configuration on the motion of the tube-forming chains and effectively dilates with t. Thus, we examined a molecular picture of *partial-DTD*[19] in which the tube dilates to the maximum possible diameter $a_{p-DTD}'(t)$ consistent with the dielectrically obtained $\varphi'(t)$ data and the Rouse-type CR dynamics, the latter activating the DTD process. For the linear/linear blends, the viscoelastic relaxation function for this partial-DTD process, $\mu_{p-DTD}(t)$, was found to be close to the $\mu(t)$ data in the entire range of t, suggesting that the DTD concept is useful if the length and time scales are consistently coarse-grained on the basis of the CR dynamics.[19]

Following the above results, we tested the validity of the partial-DTD picture for the monodisperse star PI. This test required us to know the viscoelastic CR relaxation time τ_{CR} of the monodisperse star PI. Thus, we made viscoelastic measurements for binary blends of high-M and low-M star PI chains and extrapolated the τ_{CR} data of the high-M star to its monodisperse state. The partial-DTD relaxation function $\mu_{p-DTD}(t)$, evaluated from this extrapolated τ_{CR} on the basis of the Rouse−CR dynamics for a tethered chain, was close to the $\mu(t)$ data, suggesting that the molecular picture of partial-DTD serves as a good starting point for describing the star chain dynamics with the coarse-graining treatment. Details of these results are presented in this paper.

2. Method of Test of Partial-DTD Picture

We test the partial-DTD picture for the monodisperse star chains by analyzing the star/star blend data and utilizing the Rouse−CR model. The method of this test is summarized below.

2.1. Rouse-CR Model. We consider blends of high-M star probe chains in matrices of low-M star chains. The number of the entanglement segments per arm is denoted by N_{a1} and N_{a2} for the matrix and probe, respectively. The probe chains have a small volume fraction $v_2 < N_{a2}^{-1/d}$ (with the dilation exponent $d \cong 1.3$ for PI[18]) and are entangled only with the matrix chains.

This dilute probe is expected to exhibit the Rouse-like CR relaxation if $N_{a2} \gg N_{a1}$. In the tube model for the star chains, the branching point is regarded to be fixed in space in the time scale of the viscoelastic relaxation. Then, we may utilize the Rouse dynamics for a tethered chain[1,3] (the probe arm anchored to the fixed branching point) as a good approximation and express the normalized viscoelastic CR relaxation function (normalized relaxation modulus) of the probe as

$$\mu_{CR}^{[2]}(t) = \frac{1}{N_{a2}}\left[\sum_{p=1}^{N_{a2}-N_f} \exp\left(-\frac{r_p t}{\tau_{CR}^{[2]}}\right) + \sum_{q=1}^{N_f} \exp\left(-\frac{r_q' t}{\tau_f^{[2]}}\right)\right] \quad (2)$$

with

$$r_p = \sin^2\left(\frac{\pi\{2p-1\}}{2\{2N_{a2}+1\}}\right)\sin^{-2}\left(\frac{\pi}{2\{2N_{a2}+1\}}\right) \quad (3)$$

and

$$r_q' = \sin^2\left(\frac{\pi\{2q-1\}}{2\{2N_f+1\}}\right)\sin^{-2}\left(\frac{\pi}{2\{2N_f+1\}}\right) \quad \text{with} \quad N_f \cong \sqrt{N_{a2}} \quad (4)$$

In eq 2, the first summation represents the pure CR contribution to $\mu_{CR}^{[2]}(t)$, with $\tau_{CR}^{[2]}$ and r_p (eq 3) being the longest viscoelastic CR relaxation time of the probe and a ratio of $\tau_{CR}^{[2]}$ to the relaxation time of the p-th CR mode. $\tau_{CR}^{[2]}$ increases with increasing N_{a1}, which indicates retardation of the probe motion due to the entanglement from the matrix chains. The second summation in eq 2 indicates a minor contribution from the arm length fluctuation,[1,2,8,21] as explained below.

For well entangled monodisperse stars, $\mu(t)$ partly relaxes through the shallow fluctuation of the arm length[1,15,22] (Rouse-like oscillation of the free end of the arm along the tube), and this shallow fluctuation is free from the entanglement effect (that gives an entropic penalty for the deep retraction of the arm). This fluctuation contribution, undoubtedly existing also for our dilute probe stars in star matrices, is represented by the second summation in eq 2, with $\tau_f^{[2]}$ and r_q' (eq 4) being the longest intrinsic Rouse-fluctuation time of the probe arm and a ratio of the relaxation time of $\tau_f^{[2]}$ to the q-th fluctuation mode. N_f (eq 4), specifying the upper limits of the summations in eq 2, denotes the number of entanglement segments corresponding to the fluctuation amplitude. The ratio r_q' given in eq 4 is approximate because it is formulated for a portion of the probe composed of only N_f segments. However, for the probe with $N_{a2} \gg 1$, the fluctuation contribution itself is a minor correction for the short time behavior of $\mu_{CR}^{[2]}(t)$ and the use of the approximate ratio gives no significant error in $\mu_{CR}^{[2]}(t)$ at long t.

2.2. Evaluation of Rouse—CR Parameters. In the blend with $v_2 \ll 1$, the relaxation behavior of the matrix chains is negligibly affected by the dilute probe and coincides with that in their monodisperse state. Thus, from the Rouse−CR model formulated in eqs 2−4, the complex modulus $G_b^*(\omega)$ of the blend (= Fourier transformation of the relaxation modulus) is written as a function of the angular frequency ω:

$$G_b^*(\omega) = (1-v_2)G_{1,m}^*(\omega) + \frac{v_2 G_N}{N_{a2}}\left[\sum_{p=1}^{N_{a2}-N_f} \frac{i\omega\tau_{CR}^{[2]}/r_p}{1+i\omega\tau_{CR}^{[2]}/r_p} + \sum_{q=1}^{N_f} \frac{i\omega\tau_f^{[2]}/r_q'}{1+i\omega\tau_f^{[2]}/r_q'}\right] \quad (5)$$

Here, $G_{1,m}^*(\omega)$ is the modulus of the monodisperse matrix, G_N is the entanglement plateau modulus of the blend, and $i = \sqrt{-1}$. The longest fluctuation time $\tau_f^{[2]}$ is equivalent to the intrinsic Rouse time of the probe arm and can be readily evaluated from the dielectric data[15] of linear PI chains in the nonentangled regime, and the ratios r_p and r_q' are specified by eqs 3 and 4. Thus, the only remaining parameter, $\tau_{CR}^{[2]}$, can be determined by fitting the $G_b^*(\omega)$ data of the blend with eq 5.

2.3. Partial-DTD Model for Monodisperse Star Systems. We here focus on a monodisperse system of the star chains having N_{a2} entanglement segments in each arm (identical to the probe in the blends considered earlier). The maximum number of the entanglement segments of this star that are equilibrated through the Rouse−CR motion is expressed in terms of a hypothetical CR−stress decay function $\psi_{CR}(t)$:[19]

$$\beta_{CR}(t) = \frac{1}{\psi_{CR}(t)} \quad (6)$$

Table 1. Characteristics of 6-Arm Star PI Samples

sample code[a]	$10^{-3}M_a$[b]	$10^{-3}M_w$	M_w/M_n
Low-*M* Star PI Utilized as Matrix			
6(I-09)[c]	9.5	54.2	1.05
6(I-16)[d]	16.0	95.4	1.03
6(I-24)[d]	23.5	144	1.03
6(I-31)[e]	30.6	181	1.04
6(I-41)[e]	40.7	248	1.03
High-*M* Star PI Utilized as Probe			
6(I-59)[f]	59.0	354	1.05
6(I-80)[f]	80.1	459	1.06

[a] Sample code number indicates $10^{-3}M_a$. [b] Precursor molecular weight (= arm molecular weight). [c] Synthesized/characterized in ref 23. [d] Synthesized/characterized in this study. [e] Synthesized/characterized in ref 13. [f] Synthesized/characterized in ref 15.

with

$$\psi_{CR}(t) = \frac{1}{N_{a2}}\left[\sum_{p=1}^{N_{a2}-N_f} \exp\left(-\frac{r_p t}{\tau_{CR-\epsilon}^{[2]}}\right) + \sum_{q=1}^{N_f} \exp\left(-\frac{r'_q t}{\tau_f^{[2]}}\right)\right] \quad (7)$$

The fluctuation amplitude N_f and the ratios r_p and r'_q are specified by eqs 3 and 4, and the longest fluctuation time $\tau_f^{[2]}$ is identical to that utilized in the blend. The longest CR equilibration time $\tau_{CR-\epsilon}^{[2]}$, equivalent to the dielectric CR relaxation time of the star arm having type-A dipoles and being tethered at the branching point, is twice of the viscoelastic $\tau_{CR}^{[2]}$.[19] Thus, we can experimentally determine $\tau_{CR-\epsilon}^{[2]}$ by extrapolating the viscoelastic $\tau_{CR}^{[2]}$ data in the blends to the monodisperse system.

The partial-DTD model considers that the tube dilates to the maximum possible diameter consistent with the values of the tube survival fraction $\varphi'(t)$ and the CR-equilibration number $\beta_{CR}(t)$ (eq 6). The corresponding normalized viscoelastic relaxation function is expressed as[19]

$$\mu_{p-DTD}(t) = \frac{\varphi'(t)}{\beta^*(t)} \quad \text{with} \quad \beta^*(t) = \min\left[\{\varphi'(t)\}^{-d}, \beta_{CR}(t)\right] \quad (8)$$

Here, $\{\varphi'(t)\}^{-d}$ is identical to the number $\beta_{f-DTD}(t)$ of the equilibrated segments in the full-DTD picture: The full-DTD picture is valid if the dilated tube diameter $a_{f-DTD}'(t) = a\{\beta_{f-DTD}(t)\}^{1/2}$ in this picture is smaller than the diameter $a_{CR}'(t) = a\{\beta_{CR}(t)\}^{1/2}$ allowed by the Rouse−CR mechanism, while the full-DTD picture fails if $a_{f-DTD}'(t) > a_{CR}'(t)$.

The tube survival fraction $\varphi'(t)$ is obtained from the dielectric data of the monodisperse star PI[15] with the previously reported method[19] (summarized in Appendix A of this paper), and the CR-equilibration number $\beta_{CR}(t)$ is evaluated from the viscoelastic $\tau_{CR}^{[2]}$ data in the blends (cf. eqs 6 and 7). Thus, we can experimentally determine $\mu_{p-DTD}(t)$ (eq 8) to test the partial-DTD picture by comparing this $\mu_{p-DTD}(t)$ with the $\mu(t)$ data of monodisperse star PI.

3. Experimental Section

Monodisperse 6-arm star polyisoprene (PI) samples were utilized. Two of them were synthesized in this study through coupling of living anionic linear precursor PI with 1,2-bis(trichlorosilyl)ethane,[23] and the others were synthesized in the previous studies.[13,15,23] The previously synthesized samples containing an antioxidant (butylhydroxytoluene) had been sealed with Ar and stored in a deep freezer, and the lack of chemical degradation in these samples was confirmed from GPC measurements. Table 1 summarizes the molecular characteristics of these star PI samples (determined with light scattering and GPC). The number X in the sample code 6(I−X) indicates the molecular weight of the star arm M_a in the unit of 1000.

Binary blends of the star PI samples, containing the 6(I-80) or 6(I-59) sample as a high-*M* probe component and the other samples as a low-*M* matrix component, were prepared by dissolving prescribed masses of the probe and matrix in benzene and then allowing benzene to thoroughly evaporate in vacuum. The volume fraction v_2 of the high-*M* component was kept small so that this component was entangled only with the matrix chains.

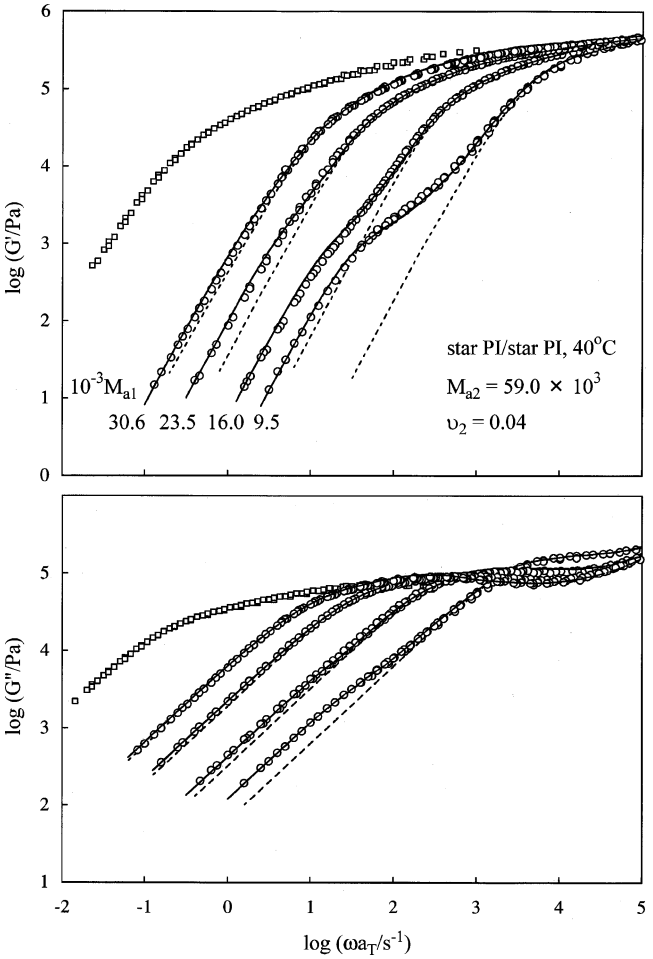

Figure 1. Linear viscoelastic moduli at 40 °C measured for star PI/star PI blends containing the 6(I-59) sample ($M_{a2} = 59.0 \times 10^3$; $N_{a2} = 12$) as the dilute probe of the volume fraction $v_2 = 0.04$ (circles). The numbers indicate $10^{-3}M_{a1}$ of the matrices. The dotted curves and squares indicate the moduli of the matrices and probe in respective monodisperse states, and the solid curves show the result of fitting with the Rouse−CR model.

For the blends thus prepared as well as for the components in respective monodisperse states, dynamic viscoelastic measurements were conducted with a laboratory rheometer (ARES, Rheometrics) in a parallel plate geometry of the diameter = 25 mm. The amplitude of the oscillatory strain was kept small (≤0.05) to ensure the linearity of the storage and loss moduli (G' and G'') measured as functions of angular frequency ω. The measurements were conducted at several temperatures between −30 and +80 °C, and master curves of G' and G'' reduced at 40 °C were constructed on the basis of time−temperature superposition. The shift factor a_T agreed excellently with that reported in the previous study.[18]

4. Results and Discussion

4.1. Overview of the Relaxation of Blends. Figures 1 and 2, respectively, show the G' and G'' data at 40 °C obtained for the blends containing the 6(I-59) and 6(I-80) samples as the dilute high-*M* probe of the volume fractions $v_2 = 0.04$ and 0.03 (circles). All matrix star chains have the arm molecular weight M_{a1} larger than M_e (= 5.0×10^3 for PI[24,25]). For comparison, the behavior of the matrices and high-*M* probes in respective monodisperse states are shown with the dotted curves and squares, respectively. The solid curves indicate the results of

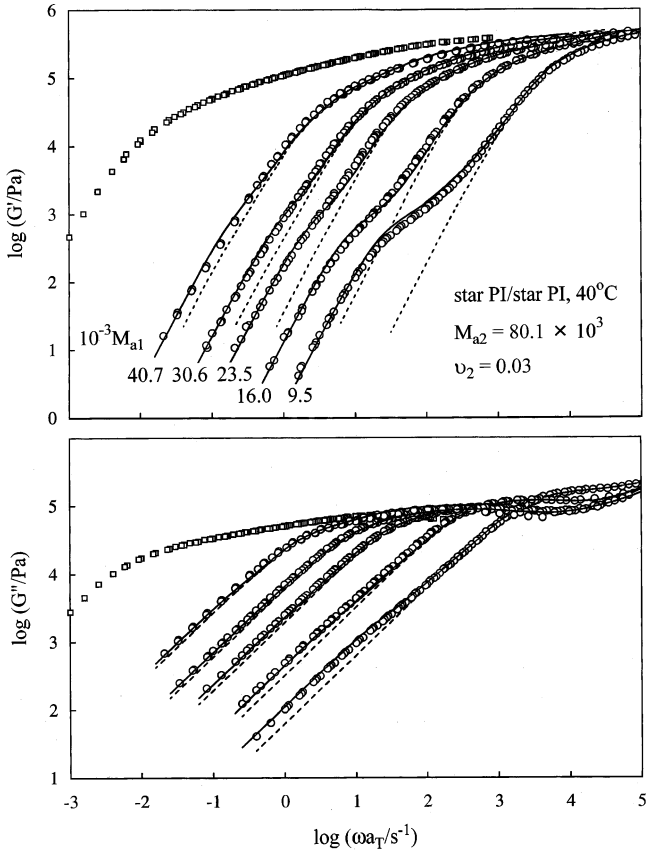

Figure 2. Linear viscoelastic moduli at 40 °C measured for star PI/star PI blends containing the 6(I-80) sample ($M_{a2} = 80.1 \times 10^3$; $N_{a2} = 16$) as the dilute probe of the volume fraction $\upsilon_2 = 0.03$ (circles). The numbers indicate $10^{-3}M_{a1}$ of the matrices. The dotted curves and squares indicate the moduli of the matrices and probe in respective monodisperse states, and the solid curves show the result of fitting with the Rouse−CR model.

fitting with the Rouse−CR model (eq 5), as explained later in more details.

In Figures 1 and 2, the G' curves of the blends clearly show the two-step relaxation.[26] The fast step is assigned as the terminal relaxation of the matrix and the early-stage relaxation of the probe, while the slow step is attributed to the terminal relaxation of the probe. The terminal relaxation of the probe becomes slower with increasing M_{a1} of the star matrix, which indicates the CR effect of the matrix on the probe relaxation. Correspondingly, the early-stage relaxation of the probe can be assigned as the onset of the CR relaxation of the probe activated by the terminal motion of the matrix. In addition, we note that the data for the blends and monodisperse matrices are indistinguishable at angular frequencies ω higher than the terminal relaxation frequency of the matrices. This result confirms that the matrix relaxation is negligibly affected by the dilute high-M chains, supporting the early argument for the model formulation (eq 5).

The reduced arm molecular weight of the high-M star probes examined in Figures 1 and 2, $\upsilon_2{}^d M_{a2} = 0.9 \times 10^3$ and 0.8×10^3 ($d = 1.3$ for PI[18]), is well below M_e ($= 5.0 \times 10^3$). Thus, these dilute probe chains should be entangled *only* with the matrix chains. This lack of probe−probe entanglements can be further examined on the basis of the blending law for the complex modulus,[18,27,28]

$$G_b^*(\omega) = (1 - \upsilon_2)\tilde{G}_{1,b}^*(\omega) + \upsilon_2\tilde{G}_{2,b}^*(\omega) \qquad (9)$$

Here, $G_b^*(\omega)$ is the modulus of the blend as a whole, and

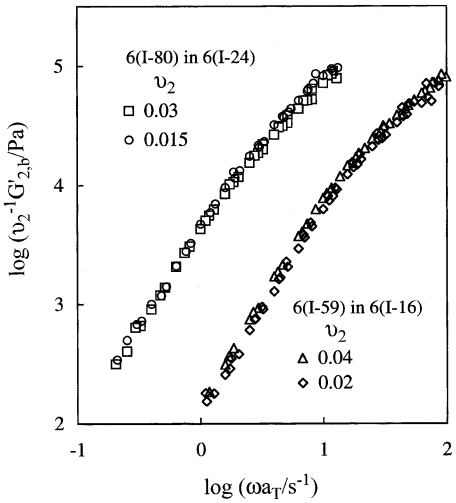

Figure 3. Comparison of the normalized storage modulus $\upsilon_2{}^{-1}G'_{2,b}(\omega)$ of the 6(I-59) and 6(I-80) probes having different volume fractions υ_2 as indicated. The good superposition of the $\upsilon_2{}^{-1}G'_{2,b}(\omega)$ data for different υ_2 values indicates that the probes at those υ_2 are dilute and entangled only with the matrix chains.

$\tilde{G}_{j,b}^*(\omega)$ is the modulus of the chain *j in the blend* normalized to unit volume fraction of this chain ($j = 1$ and 2 for the matrix and probe).

In general, $\tilde{G}_{j,b}^*(\omega)$ does not agree with the modulus of the monodisperse system of the chain j because of changes in the chain dynamics on blending. Correspondingly, the blending law (eq 9) merely states that the modulus of the blend is sustained by the matrix and probe chains. In the blends examined in Figures 1 and 2, however, the dilute probe negligibly affects the matrix relaxation and $\tilde{G}_{1,b}^*(\omega)$ can be replaced by the $G_{1,m}^*(\omega)$ data of the matrix in its monodisperse state. Then, the modulus of the probe in the blend is experimentally evaluated from the $G_b^*(\omega)$ and $G_{1,m}^*(\omega)$ data as

$$G_{2,b}^*(\omega) = G_b^*(\omega) - (1 - \upsilon_2)G_{1,m}^*(\omega) \qquad (10)$$

If the probe chains are dilute and entangled only with the matrix chains, the normalized modulus of the probe $\upsilon_2{}^{-1}G_{2,b}^*(\omega)$ ($= \tilde{G}_{2,b}^*(\omega)$ in eq 9) should be independent of υ_2.[18]

For a test of this independence, we measured $G_b^*(\omega)$ for the 6(I-81)/6(I-24) and 6(I-59)/6(I-16) blends having different probe content, $\upsilon_2 = 0.015$ and 0.03 for 6(I-80) and $\upsilon_2 = 0.02$ and 0.04 for 6(I-59). The normalized storage modulus $\upsilon_2{}^{-1}G'_{2,b}(\omega)$ evaluated from these $G_b^*(\omega)$ data (eq 10) is shown in Figure 3. (The $\upsilon_2{}^{-1}G'_{2,b}(\omega)$ data were evaluated in a range of ω where $G'_b(\omega) \geq 1.2G'_{1,m}(\omega)$ and the subtraction in eq 10 was achieved with small uncertainty.) The $\upsilon_2{}^{-1}G'_{2,b}(\omega)$ data for different υ_2 values agree with each other, confirming that the 6(I-80) and 6(I-59) probes with $\upsilon_2 = 0.03$ and 0.04 are dilute and entangled only with the matrix chains.

4.2. CR Relaxation Time of Dilute High-*M* Probe. The second-moment average relaxation time of the probe $\langle\tau^{[2b]}\rangle$, defined in terms of its relaxation spectrum $H_{2,b}(\tau)$ in the blend,[1,18,27,28] is evaluated from the $G_{2,b}^*(\omega)$ data (eq 10) as

$$\langle\tau^{[2b]}\rangle \equiv \frac{\int_{-\infty}^{\infty}\tau^2 H_{2,b}(\tau)\,d(\ln\tau)}{\int_{-\infty}^{\infty}\tau H_{2,b}(\tau)\,d(\ln\tau)} = \left[\frac{G'_{2,b}}{\omega G''_{2,b}}\right]_{\omega\to 0} \qquad (11)$$

This $\langle\tau^{[2b]}\rangle$, being identical to the product of the steady-state compliance J_e and zero-shear viscosity η_0 of the probe in the

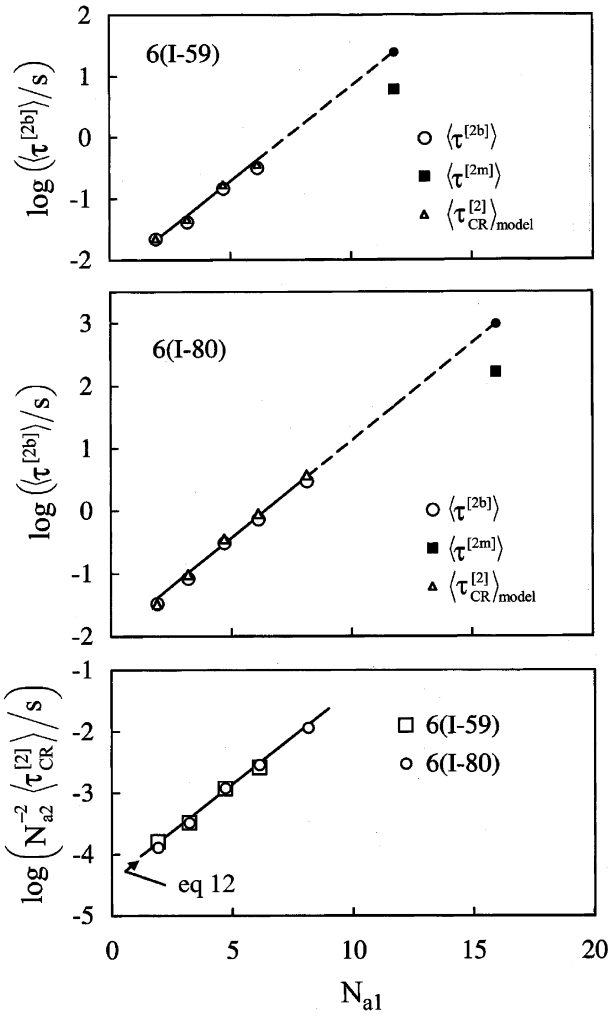

Figure 4. Top and middle panels: Semilogarithmic plots of the second-moment average viscoelastic relaxation time $\langle\tau^{[2b]}\rangle$ of the 6(I-59) and 6(I-80) probes in the blends at 40 °C against the number of the entanglement segments per arm of the matrix, N_{a1} (unfilled circles). The filled circles show the $\langle\tau^{[2b]}\rangle$ data extrapolated to the monodisperse 6(I-59) and 6(I-80) systems, and the filled squares indicate the actual $\langle\tau^{[2m]}\rangle$ data measured for these systems. The triangles indicate the relaxation time $\langle\tau_{CR}^{[2]}\rangle_{model}$ obtained from the fitting of the G_b^* data with the Rouse−CR model. Bottom panel: Semilogarithmic plots of the normalized CR relaxation time of the probes $N_{a2}^{-2}\langle\tau_{CR}^{[2]}\rangle$ against N_{a1}.

blend, weighs heavily on the slow relaxation modes (seen as the G_b' shoulder in Figures 1 and 2) and is close to the longest relaxation time of the probe. In the top and middle panels of Figure 4, the unfilled circles indicate semilogarithmic plots of $\langle\tau^{[2b]}\rangle$ of the 6(I-59) and 6(I-80) probes in the blends against the number of the entanglement segments per arm of the matrix, $N_{a1} = M_{a1}/M_e$ ($M_e = 5.0 \times 10^3$). The filled squares indicate the second-moment average relaxation time of the probe in its monodisperse system, $\langle\tau^{[2m]}\rangle$, evaluated as the product $J_e\eta_0$ of this system. The triangles show the relaxation time evaluated with the Rouse−CR model, as explained later in more details.

In the top and middle panels of Figure 4, we first note that the $\langle\tau^{[2b]}\rangle$ data in the blends (unfilled circles) are much smaller than $\langle\tau^{[2m]}\rangle$ ($\langle\tau^{[2b]}\rangle < 0.03\langle\tau^{[2m]}\rangle$). This fact unequivocally indicates that the probe motion is significantly *accelerated* by the much shorter matrix chains. Thus, the $\langle\tau^{[2b]}\rangle$ data can be utilized as the second-moment average, constraint release (CR) viscoelastic relaxation time of the probe, $\langle\tau_{CR}^{[2]}\rangle$. We also note that $\langle\tau^{[2b]}\rangle$ ($=\langle\tau_{CR}^{[2]}\rangle$) in the blends is an exponential function of N_{a1}.

Furthermore, as shown in the bottom panel of Figure 4, the normalized CR times $N_{a2}^{-2}\langle\tau_{CR}^{[2]}\rangle$ of the two probes coincide with each other and are satisfactorily described by an empirical equation shown with the solid line,

$$\langle\tau_{CR}^{[2]}\rangle = 4.0 \times 10^{-5} N_{a2}^{\ 2} \exp(0.71 N_{a1}) \quad \text{(in s)} \quad \text{at 40 °C} \tag{12}$$

(The numerical factor in the exponential term, 0.71, becomes 0.57 if we use the Doi−Edwards type entanglement spacing $M_e^{[DE]}$ ($= 4.0 \times 10^3$) in the evaluation of N_{a1}.) The N_{a2}^2 dependence of $\langle\tau_{CR}^{[2]}\rangle$ suggests the Rouse-like character of the terminal CR relaxation of the star probe in the star matrices, as also noted for the star/linear probe in linear matrices.[1,27,28] The empirical eq 12 is later utilized in our test of the partial-DTD picture.

Thus, we have obtained the $\langle\tau_{CR}^{[2]}\rangle$ data within the rigid phenomenological framework of linear viscoelasticity (eq 11). We also attempted to estimate the CR relaxation time of the probe with the other method of fitting the $G_b^*(\omega)$ data with eq 5 (Rouse−CR model). The relaxation time ratios r_p and r_q' required for the fitting were evaluated with eqs 3 and 4, and the intrinsic (entanglement-free) Rouse fluctuation amplitude (eq 4) was estimated to be $N_f \cong \sqrt{N_{a2}} \cong 3$ and 4 for 6(I-59) and 6(I-80), respectively. The remaining parameter for the fitting, the longest Rouse fluctuation time of the probe, was evaluated from the data of the dielectric relaxation time of linear PI chains[15] in the intrinsic Rouse regime as

$$10^3\tau_f^{[2]}/\text{s} = \begin{cases} 3.2 & \text{for 6(I-59)} \\ 6.3 & \text{for 6(I-80)} \end{cases} \tag{13}$$

(These $\tau_f^{[2]}$ values were obtained on the basis of a relationship between the Rouse fluctuation times of tethered and free linear chains of the same M, $\tau_f^{\text{tethered}}(M) = 4\tau_f^{\text{free}}(M)$).

Utilizing the above parameter values in eq 5, we determined the longest Rouse−CR viscoelastic relaxation time $\tau_{CR,model}^{[2]}$ that gave the best fitting of the $G_b^*(\omega)$ data of the blends. The best-fit results, shown in Figures 1 and 2 with the solid curves, are close to the data. The corresponding second-moment average relaxation time was evaluated as

$$\langle\tau_{CR}^{[2]}\rangle_{model} \equiv \left[\frac{\sum_{p=1}^{N_{a2}-N_f} r_p^{-2} + Q^2\sum_{q=1}^{N_f} r_q'^{-2}}{\sum_{p=1}^{N_{a2}-N_f} r_p^{-1} + Q\sum_{q=1}^{N_f} r_q'^{-1}}\right]\tau_{CR,model}^{[2]} \cong 0.82\tau_{CR,model}^{[2]} \tag{14}$$

where $Q = \tau_f^{[2]}/\tau_{CR,model}^{[2]}$ and r_p and r_q' are given by eqs 3 and 4. This $\langle\tau_{CR}^{[2]}\rangle_{model}$, shown with the triangles in the top and middle panels of Figure 4, agrees well with the independently determined $\langle\tau_{CR}^{[2]}\rangle$ data (unfilled circles). Thus, the viscoelastic CR relaxation time of the probe in the blends was satisfactorily determined also with the model.

4.3. CR Mode Distribution of Dilute High-*M* Probe. As seen in Figures 1 and 2, the $G_b^*(\omega)$ data of the blends are considerably well described by the Rouse−CR model for the tethered arm (eq 5). Furthermore, the second-moment average CR relaxation time $\langle\tau_{CR}^{[2]}\rangle$ is satisfactorily determined not only with the purely experimental method (eq 11) but also with the model; see Figure 4. However, these results do not guarantee that the distribution of the *fast* CR modes of the probe agrees

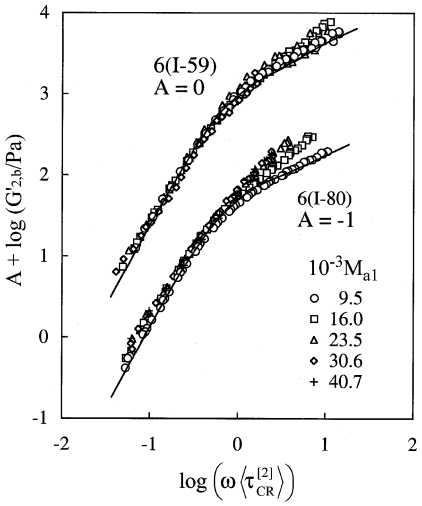

Figure 5. Plots of the storage modulus $G'_{2,b}(\omega)$ of the 6(I-59) and 6(I-80) probes in various matrices against the reduced frequency $\omega\langle\tau^{[2]}_{CR}\rangle$. The probe volume fraction is $v_2 = 0.04$ and 0.03 for 6(I-59) and 6(I-80), respectively. The plots for 6(I-80) are shifted vertically in order to avoid heavy overlapping with the plots for 6(I-59). The $\langle\tau^{[2]}_{CR}\rangle$ data utilized in the plots are shown with the unfilled circles in the top and middle panels of Figure 4.

with the Rouse distribution specified by eqs 2 and 5, because the $G^*_b(\omega)$ data at high ω are dominated by the matrix contribution (the $(1 - v_2)G^*_{1,m}(\omega)$ term in eq 5) and $\langle\tau^{[2]}_{CR}\rangle$ is insensitive to the fast modes.

The fast CR mode distribution of the probe can be most clearly examined through the ω dependence of the $G'_{2,b}$ data of the probe evaluated with eq 10. Figure 5 shows plots of the $G'_{2,b}$ data of the 6(I-59) and 6(I-80) probes in various matrices against a reduced frequency $\omega\langle\tau^{[2]}_{CR}\rangle$, with $\langle\tau^{[2]}_{CR}\rangle$ (= $\langle\tau^{[2b]}\rangle$ data) being shown with the unfilled circles in the top and middle panels of Figure 4. These $G'_{2,b}$ data were evaluated in the ranges of ω where the subtraction in eq 10 was achieved with small uncertainty. The solid curves indicate $G'_{2,b}$ of the Rouse−CR model in the 6(I-09) matrix (second term in the right-hand side of eq 5).

In the range of $\omega\langle\tau^{[2]}_{CR}\rangle$ examined in Figure 5, the $G'_{2,b}$ data of the probes in the 6(I-09) matrix (circles) are well described by the Rouse−CR model (solid curves). The model also describes the data for the terminal tail ($G'_{2,b} \propto \omega^2$) in the other matrices as well, meaning that the terminal relaxation intensity of the probe is close to that in the model ($=v_2G_N/N_{a2}$; cf. eq 5). However, for $M_{a1} \geq 16.0 \times 10^3$ ($N_{a1} > 3$), the $G'_{2,b}$ data at $\omega\langle\tau^{[2]}_{CR}\rangle > 1$ systematically deviate upward from the Rouse−CR curve with increasing N_{a1}, indicating a change in the distribution of the *fast* CR modes with N_{a1}. This change is partly related to the early stage relaxation of the probe occurring together with the terminal relaxation of the matrix, as discussed below.

As seen in eqs 2 and 5, the slowest and fastest CR modes considered in the model have the relaxation times $\tau^{[2]}_{slowCR} = \tau^{[2]}_{CR}$ and $\tau^{[2]}_{fastCR} = \tau^{[2]}_{CR}/r^*_p$ with $p^* = N_{a2} - N_f$, respectively. In the top and bottom panels of Figure 6, ratios of these times to the matrix relaxation time $\langle\tau^{[1]}\rangle$ (= $J_e\eta_0$ for the matrix) are plotted against N_{a1}. As seen in the top panel, the $\tau^{[2]}_{slowCR}/\langle\tau^{[1]}\rangle$ ratio strongly decreases with increasing N_{a1}. This decrease can be noted also in Figures 1 and 2; see the decrease of the width the low-ω shoulder of the G'_b data with increasing N_{a1}. Thus, the interval between the early and terminal stages of CR relaxation of the probe, the former occurring together with the matrix relaxation at $\omega \sim 1/\langle\tau^{[1]}\rangle$, is considerably narrow for large N_{a1}.

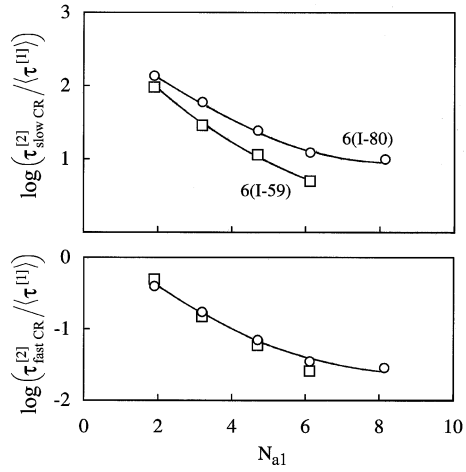

Figure 6. Top panel: N_{a1} dependence of the ratio of $\tau^{[2]}_{slowCR}$ for the slowest CR mode of the dilute 6(I-59) and 6(I-80) probes to the matrix relaxation time $\langle\tau^{[1]}\rangle$. Bottom panel: N_{a1} dependence of the ratio of $\tau^{[2]}_{fastCR}$ for the fastest CR mode of the dilute 6(I-59) and 6(I-80) probes considered in the Rouse−CR model to $\langle\tau^{[1]}\rangle$.

Corresponding to this narrowness, the $\tau^{[2]}_{fastCR}/\langle\tau^{[1]}\rangle$ ratio for the Rouse−CR model becomes much smaller than unity for large N_{a1} (cf. bottom panel of Figure 6) and thus the fast CR modes considered in the model occurs much earlier than the terminal relaxation of the matrix. However, the actual fast CR modes of the probe are activated by the matrix motion and should be delayed until the time scale of the matrix relaxation. This delay, being more significant in higher-N_{a1} matrices, leads to the systematic upward deviation of the $G'_{2,b}$ data at $\omega\langle\tau^{[2]}_{CR}\rangle > 1$ (Figure 5).

The simple Rouse−CR model does not consider this delay and underestimates the relaxation times of the fast CR modes. (A similar problem, though much less prominent, is noted also in linear matrices.[1]) In addition, the entanglement in the star matrices would have a broadly distributed lifetime that reflects the broad distribution of the motional modes of the matrix arms. The expressions of $\mu^{[2]}_{CR}(t)$ and $G^*_b(\omega)$ for the Rouse−CR model (eqs 2 and 5) need to be convoluted with respect to this lifetime distribution.[29]

Despite these problems of the simple Rouse−CR model, this model describes the $G'_{2,b}$ data for the terminal tail of all blends examined (Figure 5) and appears to work for the slow CR modes determining this tail. In addition, the CR relaxation time evaluated from the fitting with the model is satisfactorily close to the time independently determined with the purely experimental method (cf. top and middle panels of Figure 4). For these reasons, we use the simple Rouse−CR model in the test of the partial-DTD picture described below.

4.4. Test of Partial-DTD Picture for High-*M* Monodisperse Stars. In this section, we examine the DTD picture for monodisperse systems of 6(I-59) and 6(I-80). For this purpose, we extrapolated the $\langle\tau^{[2]}_{CR}\rangle$ data of 6(I-59) and 6(I-80) in the blends to their monodisperse systems with the aid of eq 12 to estimate the second-moment average, Rouse−CR viscoelastic relaxation time in these systems, $\langle\tau^{[2m]}_{CR}\rangle$ = 24 and 890 s for 6(I-59) and 6(I-80), respectively. These estimates, shown with the filled circles in the top and middle panels of Figure 4, are larger than the measured relaxation times of the monodisperse systems (filled squares) only by factors of 4.0 and 5.4 for 6(I-59) and 6(I-80), respectively. This result suggests that the CR mechanism largely contributes to the terminal relaxation of the monodisperse star PI. A similar result was also noted for polystyrene stars.[1,30]

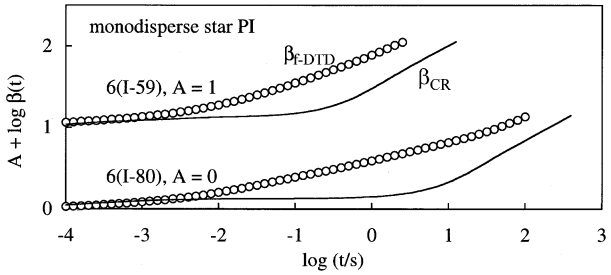

Figure 7. Comparison of the number of CR-equilibrated entanglement segments β_{CR} (solid curves) with the full-DTD equilibration number β_{f-DTD} (circles) for 6(I-59) and 6(I-80) in respective monodisperse states at 40 °C. The plots for 6(I-59) are shifted vertically to avoid heavy overlapping with the plots for 6(I-80).

With the aid of eq 14, the longest Rouse−CR viscoelastic relaxation time in the monodisperse systems $\tau_{CR}^{[2m]}$ is obtained from the above $\langle\tau_{CR}^{[2m]}\rangle$ values: $\tau_{CR}^{[2m]} = \langle\tau_{CR}^{[2m]}\rangle/0.82 = 29$ and 1090 s for 6(I-59) and 6(I-80), respectively. Utilizing the corresponding Rouse−CR equilibration time $\tau_{CR-\epsilon}^{[2m]} = 2\tau_{CR}^{[2m]}$ and the intrinsic Rouse fluctuation time $\tau_f^{[2]}$ (eq 13) in eqs 6 and 7, we evaluated the number of the entanglement segments mutually equilibrated through the Rouse−CR mechanism, $\beta_{CR}(t)$. Figure 7 compares this $\beta_{CR}(t)$ with the full-DTD equilibration number $\beta_{f-DTD}(t)$ evaluated dielectrically in the previous study.[15] (The comparison is made in the range of $\beta < N_{a2}$ where the DTD picture has a sound meaning.) Clearly, $\beta_{CR}(t)$ is significantly smaller than $\beta_{f-DTD}(t)$ at $t > 0.1$ s where the dominant part of the terminal relaxation occurs in the monodisperse 6(I-59) and 6(I-80) systems. This fact is indicative of the incomplete CR equilibration over the length scale of $a_{f-DTD}'(t) = a\{\beta_{f-DTD}(t)\}^{1/2}$ assumed in the full-DTD picture and naturally leads to the failure of this picture.[15] For the same reason, the full-DTD molecular model[8] cannot give a *consistent* description of the dielectric and viscoelastic data of monodisperse star PI, as shown in Appendix B.

For the monodisperse 6(I-59) and 6(I-80) systems, the tube survival fraction $\varphi'(t)$ is evaluated from the dielectric data[15] with the previous method[19] summarized in Appendix A. Utilizing the $\varphi'(t)$ data (shown in Appendix A) and the $\beta(t)$ data (Figure 7) in eq 8, we evaluated the viscoelastic relaxation function for the partial-DTD picture, $\mu_{p-DTD}(t)$. Figure 8 compares this $\mu_{p-DTD}(t)$ (solid curves) with the $\mu(t)$ data (circles). For comparison, $\mu_{f-DTD}(t)$ for the full-DTD picture (reported previously in the form of G' and G'') is shown with the dotted curve. The $\mu_{f-DTD}(t)$ is considerably smaller than the $\mu(t)$ data in the terminal relaxation regime, confirming the failure of the full-DTD picture. In contrast, $\mu_{p-DTD}(t)$ is close to the $\mu(t)$ data in the entire range of t, suggesting that the partial-DTD picture works considerably well for the monodisperse star chains.

However, in Figure 8, we also note small but nonnegligible differences between $\mu_{p-DTD}(t)$ and $\mu(t)$. Thus, the simplest partial-DTD picture based on the Rouse−CR dynamics of the tethered chain (eqs 2 and 6−8) is to be modified for several points not considered in this dynamics. In particular, the modification should be made for the interval between the early and terminal stages of the CR relaxation and the distribution of the entanglement lifetime, as discussed earlier for the CR mode distribution in the blends. In addition, a motional correlation of the arms of each star chain might need to be incorporated in the model. These modifications, expected to improve the agreement between the calculated $\mu_{p-DTD}(t)$ and measured $\mu(t)$, are an important subject of future theoretical studies.

Despite this problem, the partial-DTD picture enables us to make a consistent description of the viscoelastic and dielectric data of the monodisperse star PI, the latter giving the tube survival fraction. This picture is based on the self-consistent coarse-graining of the length and time scales, and a more detailed description of the star dynamics could be made without the coarse-graining, i.e., by using the entanglement segment as the motional unit in any time scale. This description requires us to formulate a time evolution equation of the positions of those segments that incorporates all details of the CR dynamics including its non-Rouse aspect,[1] but these details have not been fully elucidated yet. In addition, for branched chains having trunks and arms (such as the pom-poms and combs), this time evolution equation would become intractably complicated because of the large difference in the relaxation rates of the trunks and arms. From this point of view, the simple partial-DTD picture would serve as a good starting point for describing the entanglement dynamics of the branched chains with various topologies.[31]

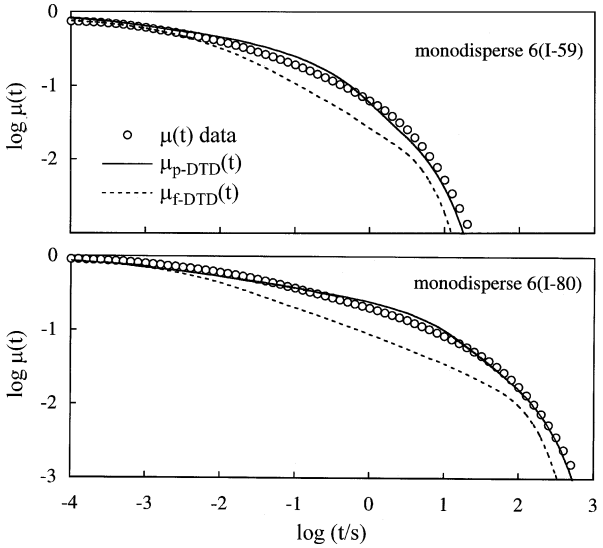

Figure 8. Comparison of the normalized viscoelastic relaxation function for the partial-DTD process $\mu_{p-DTD}(t)$ (solid curves) with the $\mu(t)$ data (circles) for the monodisperse 6(I-59) and 6(I-80) systems at 40 °C. The dotted curves indicate $\mu_{f-DTD}(t)$ for the full-DTD picture.

5. Concluding Remarks

We have examined the linear viscoelastic behavior of star PI/star PI binary blends and detected the CR relaxation of the dilute probe in much shorter matrices. The terminal CR relaxation time of the probe, described by an empirical equation $\langle\tau_{CR}^{[2]}\rangle/s \cong 4.0 \times 10^{-5} N_{a2}^2 \exp(0.71 N_{a1}) \propto N_{a2}^2$, was consistent with the simplest Rouse−CR model for the tethered arm, although the distribution of the fast CR modes in matrices of fairly large N_{a1} was different from that of the model possibly because the model did not properly account for the interval between the early and terminal stages of actual CR relaxation and the distribution of the entanglement lifetime.

On the basis of these results for the blends, we have tested the validity of the partial-DTD picture for monodisperse, high-M star PI. The viscoelastic relaxation function deduced from this picture, $\mu_{p-DTD}(t)$, was close to the $\mu(t)$ data, suggesting that the partial-DTD picture serves as a good starting point for describing the entanglement dynamics of the stars and other types of branched chains.

Acknowledgment. This study was partly supported by Grant-in-Aid for Scientific Research from JSPS (Grant No. 17350108).

CDV

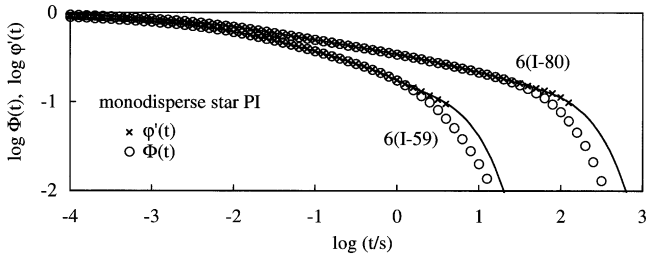

Figure 9. Survival fraction of the dilated tube $\varphi'(t)$ (crosses) evaluated from the dielectric $\Phi(t)$ data (circles) for the monodisperse 6(I-59) and 6(I-80) systems at 40 °C.

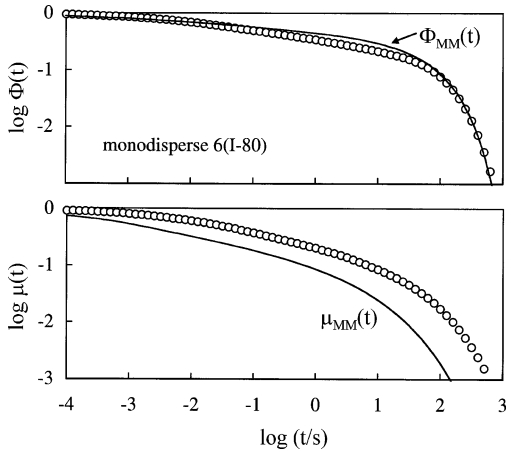

Figure 10. Comparison of the dielectric $\Phi(t)$ and viscoelastic $\mu(t)$ data for the monodisperse 6(I-80) system at 40 °C with $\Phi_{MM}(t)$ and $\mu_{MM}(t)$ deduced from the Milner−McLeish model. The local friction coefficient included in the model was determined by fitting the $\Phi(t)$ data with the model.

Appendix A. Dielectric Determination of Tube Survival Fraction

For the star chains having type-A dipoles parallel to the arms, the normalized dielectric relaxation function $\Phi(t)$ is equivalent to the autocorrelation function of the end-to-end vector of the arm.[15,16,32] For the arm composed of N_a entanglement segments and tethered to a fixed branching point, a simple geometrical analysis gives a general relationship between the tube survival fraction $\varphi'(t)$ and the dielectric $\Phi(t)$ data:[15,17,19]

$$\varphi'(t) = \Phi(t) + \frac{1}{8N_a}\left[\frac{a'(t)}{a} - 1\right]^2 \qquad \text{(A1)}$$

Here, the second term in the right-hand side indicates a correction for the fluctuation of the arm at the edge of a surviving portion of the tube having the dilated diameter $a'(t)$ at time t.

In the partial-DTD picture, the $a'(t)/a$ ratio appearing in eq A1 is specified as[19]

$$\frac{a'(t)}{a} = \{\beta^*(t)\}^{1/2} \quad \text{with} \quad \beta^*(t) = \min[\{\varphi'(t)\}^{-d}, \beta_{CR}(t)] \qquad \text{(A2)}$$

Here, $\beta_{CR}(t)$ is the Rouse−CR equilibration number of the entanglement segments (shown in Figure 7 with the solid curves), and the factor $\{\varphi'(t)\}^{-d}$ ($d = 1.3$ for PI[18]) is identical to the equilibration number $\beta_{f-DTD}(t)$ for the full-DTD process.

Combining eqs A1 and A2, we evaluated $\varphi'(t)$ from the $\Phi(t)$ data for the monodisperse 6(I-59) and 6(I-80) systems obtained in the previous study.[15] The evaluation was limited in a range of t where the size of the dilated segment is smaller than that of the arm as a whole ($\beta^*(t) < N_a$) and the DTD picture has a sound meaning. In Figure 9, the $\varphi'(t)$ data thus evaluated (crosses) are compared with the dielectric $\Phi(t)$ data (circles). The $\varphi'(t)$ is close to $\Phi(t)$ until the terminal dielectric relaxation occurs, and $\varphi'(t)$ becomes a little larger than $\Phi(t)$ in the terminal regime where the tube has dilated significantly and the tube-edge correction in eq A1 has a nonnegligible contribution to $\varphi'(t)$. These $\varphi'(t)$ data were fitted with a sum of exponential decaying terms, as shown with the solid curves. These fitting functions, well describing the available $\varphi'(t)$ data, were utilized in the test of the partial-DTD picture (Figure 8).

Appendix B. Comparison of MM Model with $\mu(t)$ Data

For PI star chains having the dipoles parallel to their arms, the normalized viscoelastic and dielectric relaxation functions $\mu_{MM}(t)$ and $\Phi_{MM}(t)$ deduced from the full-DTD model by Milner and McLeish[8] (MM) can be written as[15]

$$\mu_{MM}(t) = (d+1)\int_0^1 (1-s)^d \exp\left(-\frac{t}{\tau_{MM}(s)}\right) ds \qquad \text{(B1)}$$

and

$$\Phi_{MM}(t) = \frac{1}{K}\int_0^{1-(1/N_a)} \left[1 + \frac{d}{8N_a}\{(1-s)^{-(d+1)} - (1-s)^{-(d+1/2)}\}\right] \exp\left(-\frac{t}{\tau_{MM}(s)}\right) ds \qquad \text{(B2)}$$

Here, s is the normalized curvilinear coordinate of the entanglement segments in the star arm, d is the dilation exponent ($d \cong 1.3$ for PI[18]), and K is a normalization constant ensuring $\Phi(0) = 1$. The relaxation time of the segment having the coordinate s, $\tau_{MM}(s)$, is given as a combination of the relaxation times for the shallow Rouse-like fluctuation and deep retraction of the arm,[8] the latter associated with the entropic penalty.

In the top panel of Figure 10, the dielectric $\Phi(t)$ data of the monodisperse 6(I-80) system obtained in the previous study (circles) is fitted with the MM model (eq B2; shown with the solid curve). With an appropriate choice of a value of the local friction coefficient ζ included in $\tau_{MM}(s)$, the fitting is achieved satisfactorily. However, as shown in the bottom panel, $\mu_{MM}(t)$ for the same ζ value (curve) is significantly smaller than the $\mu(t)$ data (circles) at long t. If the ζ value is determined from the fitting for the $\mu(t)$ data, $\Phi_{MM}(t)$ becomes larger than the $\Phi(t)$ data, as shown previously for the dielectric loss ϵ'' (= Fourier transformation of Φ). These results indicate that the full-DTD picture cannot make a consistent description of the dielectric and viscoelastic data of star PI even with the most elaborated treatment in the MM model. In contrast, $\mu_{p-DTD}(t)$ evaluated from the dielectric $\Phi(t)$ data (that give the tube survival fraction; cf. Appendix A) is close to the $\mu(t)$ data (cf. Figure 8), demonstrating that the partial-DTD picture can make the consistent description.

References and Notes

(1) Watanabe, H. *Prog. Polym. Sci.* **1999**, *24*, 1253.
(2) McLeish, T. C. B. *Adv. Phys.* **2002**, *51*, 1379.
(3) Graessley, W. W. *Adv. Polym. Sci.* **1982**, *47*, 67.
(4) Likhtman, A. E.; McLeish, T. C. B. *Macromolecules* **2002**, *36*, 6332.
(5) Graham, R. S.; Likhtman, A. E.; McLeish, T. C. B. *J. Rheol.* **2003**, *47*, 1171.
(6) Marrucci, G. J. *Polym. Sci. Polym. Phys. Ed.* **1985**, *23*, 159.
(7) Ball, R. C.; McLeish, T. C. B. *Macromolecules* **1989**, *22*, 1911.
(8) Milner, S. T.; McLeish, T. C. B. *Macromolecules* **1997**, *30*, 2159; **1998**, *31*, 7479.
(9) Milner, S. T.; McLeish, T. C. B. *Phys. Rev. Lett.* **1998**, *81*, 725.

(10) Milner, S. T.; McLeish, T. C. B.; Young, R. N.; Hakiki, A.; Johnson, J. M. *Macromolecules* **1998**, *31*, 9345.
(11) Park, S. J.; Larson, R. G. *Macromolecules* **2004**, *27*, 597.
(12) Matsumiya, Y.; Watanabe, H.; Osaki, K. *Macromolecules* **2000**, *33*, 499.
(13) Watanabe, H.; Matsumiya, Y.; Osaki, K. *J. Polym. Sci., Part B: Polym. Phys.* **2000**, *38*, 1024.
(14) Matsumiya, Y.; Watanabe, H. *Macromolecules* **2001**, *34*, 5702.
(15) Watanabe, H.; Matsumiya, Y.; Inoue, T. *Macromolecules* **2002**, *35*, 2339.
(16) Watanabe, H. *Macromol. Rapid Commun.* **2001**, *22*, 127.
(17) Watanabe, H. *Kor.-Austr. Rheol. J.* **2001**, *13*, 205.
(18) Watanabe, H.; Ishida, S.; Matsumiya, Y.; Inoue, T. *Macromolecules* **2004**, *37*, 1937.
(19) Watanabe, H.; Ishida, S.; Matsumiya, Y.; Inoue, T. *Macromolecules* **2004**, *37*, 6619.
(20) Frischknecht. A. L.; Milner, S. T. *Macromolecules* **2000**, *33*, 9764.
(21) Doi, M.; Edwards, S. F. *The Theory of Polymer Dynamics*; Clarendon: Oxford, U.K., 1986.
(22) Fetters, L. J.; Kiss, A. D.; Pearson, D. S.; Quack, G. F.; Vitus, F. J. *Macromolecules* **1993**, *26*, 647.
(23) Yoshida, H.; Adachi, K.; Watanabe, H.; Kotaka, T. *Polym. J.* **1989**, *21*, 863.
(24) Ferry, J. D. *Viscoelastic Properties of Polymers*, 3rd ed.; Wiley: New York, 1980.
(25) Graessley, W. W. *Adv. Polym. Sci.* **1974**, *16*, 1.
(26) The terminal relaxation of the dilute probes is not well resolved as a shoulder in the G'' data because G'' is insensitive to slow and weak relaxation modes. Nevertheless, the G'' data of the blends are larger than those of the monodisperse matrices at low ω (cf. Figures 1 and 2), demonstrating the contribution of the dilute high-M probe to G'' of the blends.
(27) Watanabe, H.; Sakamoto, T.; Kotaka, T. *Macromolecules* **1985**, *18*, 1436.
(28) Watanabe, H.; Kotaka, T. *Macromolecules* **1986**, *19*, 2520.
(29) Rubinstein, M.; Colby, R. H. *J. Chem. Phys.* **1988**, *89*, 5291.
(30) Watanabe, H.; Yoshida, H.; Kotaka, T. *Macromolecules* **1992**, *25*, 2442.
(31) (a) Yaoita and co-workers[31b] made a molecular simulation based on the full-DTD picture for monodisperse linear chains (that are known to obey this picture).[12,15−17] This picture enabled a very fast simulation with a high accuracy, demonstrating the usefulness of the DTD concept in numerical studies of entanglement dynamics. For the star chains not obeying the full-DTD picture, the fast simulation could be still made on the basis of the partial-DTD picture. This simulation is considered as an important subject of future work. (b) Yaoita, T.; Isaki, T.; Masubuchi, Y.; Watanabe, H.; Ianniruberto, G.; Greco, F.; Marrucci, G. *J. Chem. Phys.* **2004**, *121*, 12650.
(32) Riande, E.; Saiz, E. *Dipole Moments and Birefringence of Polymers*; Prentice Hall: Englewood Cliffs, NJ, 1992.

MA0600198